Ceramics International 43 (2017) 6425–6429

Contents lists available at ScienceDirect

Ceramics International

journal homepage: www.elsevier.com/locate/ceramint

Phase formation of $(Y,Ce)_2BaAl_4SiO_{12}$ yellow microcrystal-glass phosphor for blue LED pumped white lighting

Haipeng Ji[a,b], Yujin Cho[b,c], Le Wang[d,*], Naoto Hirosaki[b], Maxim S. Molokeev[e,f], Zhaohui Huang[a,**], Rong-Jun Xie[b,g,***]

[a] Beijing Key Laboratory of Materials Utilization of Nonmetallic Minerals and Solid Wastes, National Laboratory of Mineral Materials, School of Materials Science and Technology, China University of Geosciences (Beijing), Beijing 100083, China
[b] Sialon Group, National Institute for Materials Science, 1-1 Namiki, Tsukuba 305-0044, Japan
[c] Nano Device Characterization Group, National Institute for Materials Science, 1-1 Namiki, Tsukuba 305-0044, Japan
[d] College of Optical and Electronic Technology, China Jiliang University, Hangzhou 310018, China
[e] Laboratory of Crystal Physics, Kirensky Institute of Physics, Federal Research Center KSC SB RAS, Krasnoyarsk 660036, Russia
[f] Department of Physics, Far Eastern State Transport University, Khabarovsk, 680021, Russia
[g] College of Materials, Xiamen University, Xiamen, China

ARTICLE INFO

Keywords:
Phosphor
WLED
Photoluminescence
Cathodoluminescence

ABSTRACT

The $(Y,Ce)_2BaAl_4SiO_{12}$ phosphor, a garnet-structured blue-to-yellow color convertor for WLED, exhibits an interesting "microcrystal-glass powder" feature, which can be regarded as the 4th form for phosphor, in addition to the "ceramic powder phosphor", the "single crystal phosphor" and the "glass-ceramic phosphor". The structure exhibits luminescent microcrystals embedding in non-luminescent glass matrix: the spherical crystals are mainly arranged around the glass phase forming a "necklace" pattern, while the individual crystals show a "core-shell" architecture regarding the luminescence intensity variation. Further combining the phase evolution evidence evaluated by Rietveld refinement, we propose the formation mechanism for such unique morphology/structure as a two-stage process, including an initial nucleation by solid state reaction and following liquid-assisted crystal growth, instead of a precipitation-crystallization process.

1. Introduction

Phosphor materials play a key role in the phosphor-converted white light emitting diode (WLED) lamps, determining several critical parameters such as luminous efficacy, color rendering and color temperature [1–3]. Recently, we reported a solid solution phosphor series of $Y_2MAl_4SiO_{12}:Ce^{3+}$ (M=Ba, Sr, Ca, Mg) created from $Y_3Al_5O_{12}:Ce^{3+}$ using a polyhedron substitution strategy [4,5], where YO_8 and AlO_4 are partially replaced by MO_8 and SiO_4, respectively. These artificial garnets use less rare earth and require lower synthesis temperature than the starting $Y_3Al_5O_{12}$:Ce, which thus, reduce the production cost [6]. Moreover, this series show interesting morphology/structure favorable for the title phosphor to be employed in a phosphor-in-glass packaging: besides the crystalline garnet phase, a glass phase is observed, the ratio of which depends both on the cation type (of M) and the substitution level designed in $Y_{3-x}M_xAl_{5-x}Si_xO_{12}$:Ce ($0 < x < 1$). For M=Ba, the yellow-emitting microcrystals embed in the glass matrix within the individual powder particles [6], forming a unique feature which distinguishes it from the conventional "ceramic powder phosphor", "single crystal phosphor" or "glass-ceramic phosphor". For the phosphor-in-glass preparation, such microcrystal-glass morphology can protect the phosphor particles from heat attack during co-sintering with the glass frit; besides, this feature may be also promisingly applicable for the preparation of glass-ceramic phosphor. Furthermore, $Y_2BaAl_4SiO_{12}$:Ce exhibits a relatively high emission stability against thermal quenching [6], making it favorable for application in high-power WLED.

Currently, the formation mechanism of such interesting crystal-glass co-existing feature in $Y_2BaAl_4SiO_{12}$:Ce remains to be unclear. In this study, we further vary the synthesis on aspects of heating temperature, holding period and cooling rate; the phase composition, micromorphology, point-dependent cathodoluminescence emission and element distribution at micro areas were characterized to reveal the phase formation mechanism. A two-stage process including an

* Corresponding author at: College of Optical and Electronic Technology, China Jiliang University, Hangzhou 310018, China.
** Corresponding author at: School of Materials Science and Technology, China University of Geosciences (Beijing), Beijing 100083, China.
*** Corresponding author at: Sialon Group, National Institute for Materials Science, 1-1 Namiki, Tsukuba 305-0044, Japan.
E-mail addresses: calla@cjlu.edu.cn (L. Wang), huang118@cugb.edu.cn (Z. Huang), XIE.Rong-Jun@nims.go.jp, rjxie@xmu.edu.cn (R.-J. Xie).

http://dx.doi.org/10.1016/j.ceramint.2017.02.055
Received 26 December 2016; Received in revised form 23 January 2017; Accepted 11 February 2017
Available online 13 February 2017

initial nucleation by solid state reaction at a relatively low temperature followed by liquid-assisted crystal growth at elevated temperature was proposed, as a more reasonable formation mechanism than a precipitation-crystallization hypothesis, to explain the observed architecture between the crystalline and glass phases. Such understanding may benefit for the composition design, synthesis optimization and morphology tuning when developing new microcrystal-glass type phosphors.

2. Experimental procedure

The Ce-doped $Y_2BaAl_4SiO_{12}$ phosphors were prepared via the reaction $Y_2O_3+BaCO_3+2Al_2O_3+SiO_2+CeO_2 \rightarrow Y_2BaAl_4SiO_{12}:Ce +CO_2\uparrow$ by firing the powder mixtures of Y_2O_3, CeO_2, $BaCO_3$, Al_2O_3, SiO_2 (purity > 99.9%) in stoichiometric ratios to form the nominal composition of $Y_{1.92}Ce_{0.08}BaAl_4SiO_{12}$. The mixtures were compacted into pellets in a steel mould by hand and then placed in BN crucibles, which were fired in a horizontal tube furnace under flowing H_2(5%)-N_2(95%) atmosphere. The pellet samples, instead of powder samples, were preferred, since we want to observe the microstructure on the fresh fractured surface and to perform the cathodoluminescence mapping on fractured crystal-glass phases. After sintering, the pellet products were cracked and the microstructure of the fracture surfaces were observed on a scanning electron microscope (SEM; S4300, Hitachi, Japan) equipped with a cathodoluminescence system (CL; MP32S/M, Horiba, Japan). The beam current of the CL analysis was fixed at 100 pA and the electron beam energy was set at 5 kV, which accordingly corresponds to a penetration depth of about 350 nm. The composition of a micro area was determined by energy-dispersive X-ray spectroscopy (EDS; EMAX Evolution, Horiba, Japan) equipped on an SEM (S-4800, Hitachi, Japan). Phase composition was studied on an X-ray diffractometer (XRD; Smartlab, Rigaku, Tokyo, Japan) with CuK_α radiation (1.54056 Å), operating at 45 kV and 200 mA and using a scan speed of 2°/min. Photoluminescence spectra were measured at room temperature using a spectrofluorometer (FP-6500, Jasoc, Japan).

3. Results and discussion

In our previous study, the cathodoluminescence mapping (for the 540 nm emission) on the cross-sectional area of individual particles of $Y_2BaAl_4SiO_{12}$:Ce powder sample shows isolated microcrystals uniformly embedding in the non-luminescent matrix [6]. One formation hypothesis for such structure is the precipitation of luminescent microcrystals from the glass melt during the heating process, similarly with that in the glass-ceramic phosphor formation. However, further study on the fracture surfaces of the pellet samples also demonstrates the arrangement of luminescent microcrystals around a glass “core” in a ring-pattern instead of being inside of this glass phase. Therefore, the precipitation-crystallization mechanism is unable to well explain all the observed architecture between the luminescent microcrystals and the non-luminescent glass phase; probably, alternative mechanism should be proposed.Here, two sets of synthesis were comparatively designed: the first set were fired at 1400 °C for 2 h (the parameter of 1400 °C for 2 h was chosen since the $Y_{1.92}Ce_{0.08}BaAl_4SiO_{12}$ powder sample formed single crystalline phase under such condition [6]) with different cooling rates (in the stage from 1400 to 1000 °C) fixed as 10, 5, or 1 °C/min, respectively; another set were fired at 1400 or 1350 °C for different holding periods of 1 min, 30 min, 1 h, 2 h, 4 h or 6 h with fixed cooling rate of 5 °C/min (in the stage from 1400 to 1000 °C). When the temperature decreased to be below 1000 °C, the furnace was turned off and the samples were cooled down therein naturally. Such preparation schedules are illustrated in Fig. 1. As seen from the digital images, the volume shrinkages of the pellet samples are seen to be quite different from each other, suggesting different phase formations. Most of the pellets show bright yellow emission under sunlight.

For the precipitation hypothesis where crystals form when the solution becomes supersaturated with respect to some compounds during cooling, the cooling rate may affect the crystal size: a rapid cooling generally obtains many small crystals; while, a slower cooling encourages fewer well-grown bigger crystals. Thus, the effect of cooling rate is firstly examined. Fig. S1a shows the XRD patterns and photoluminescence excitation (PLE) and photoluminescence emission (PL) spectra of the samples a, b, and c with varying cooling rates. Different from the powder synthesis which produced pure garnet phase by heating at 1400 °C for 2 h followed with natural cooling, the pellet synthesis after heating at 1400 °C for 2 h generates the garnet main phase together with some residue $BaAl_2O_4$. With decreasing cooling rate, the intensity of the diffraction peaks gradually gets enhanced (under the same XRD collecting conditions such as exposition time) (Fig. S1a), suggesting less remaining glass and higher crystallinity. Besides, the relative amount of the two crystalline phases was roughly estimated by Rietveld refinement using TOPAS 4.2 [7], which shows garnet/$BaAl_2O_4$ weight ratios of 90.6(2.4)%/9.4(2.4)% for sample a (CR=10 °C/min), 91.6(1.6)%/8.4(1.6)% for b (CR=5 °C/min), and 91.7(1.5)%/8.3(1.5)% for c (CR=1 °C/min). Thus, the cooling rate has a slight effect on the phase composition, and CR=5 or 1 °C/min generated the pellet with a slightly high garnet portion. The PLE/PL spectra of samples a, b, and c are almost identical with maximums at 454 and 537 nm, respectively (Fig. S1b).

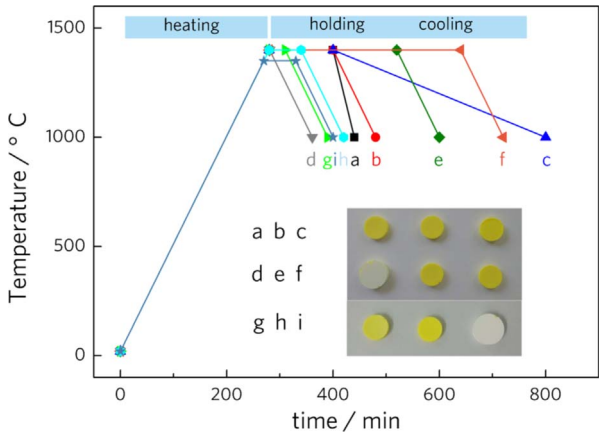

Fig. 1. Preparation schedules designed to study the effects of heating temperature (T), holding period (t) and cooling rate (CR) on the formation of $(Y,Ce)_2BaAl_4SiO_{12}$ microcrystal-glass phosphor. With T=1400 °C and t=2 h, samples a, b, and c have CR of 10, 5, and 1 °C/min, respectively; with CR =5 °C/min and T=1400 °C, samples d to h have t of 1 min, 4 h, 6 h, 30 min, 1 h, respectively; sample i have T=1350 °C, t=1 h and CR =5 °C/min. The insert shows the digital image of as-prepared pellet samples.

The microstructure of the samples a and c were then observed (Fig. 2). The surfaces contain two distinct features corresponding to the fractures of respective crystals and glass: the fracture of glass left smoother surface while that of crystals generated coarser holes. However, both the microstructure and CL mapping results do not reveal any clear effect of cooling rate on crystal size: most of the luminescent crystals in samples a and c are of similar size in the range of 0.5–2 μm. Interestingly, one can see that the spherical luminescent microcrystals generally tend to be arranged in a “necklace” pattern surrounding the inner non-luminescent glass phase (see highlighted marks in CL mapping of Fig. 2). Such architecture suggests a mechanism of liquid phase assisted ion diffusion favorable for the crystal growth; the microcrystals surrounding the glass “core” may be induced by the surface tension energy of the liquid at high temperature. Furthermore, the “core” of the “necklace” is non-luminescent free from garnet crystal formation, which is against the hypothesis of crystal-precipitation from supersaturated solution during cooling.

Since the CR of 5 °C/min encourages a high garnet/$BaAl_2O_4$ ratio which also causes less harm to furnace than quenching CR of 10 °C/min or spends much less time than CR of 1 °C/min, the following synthesis variations on T or t were conducted with CR of 5 °C/min,

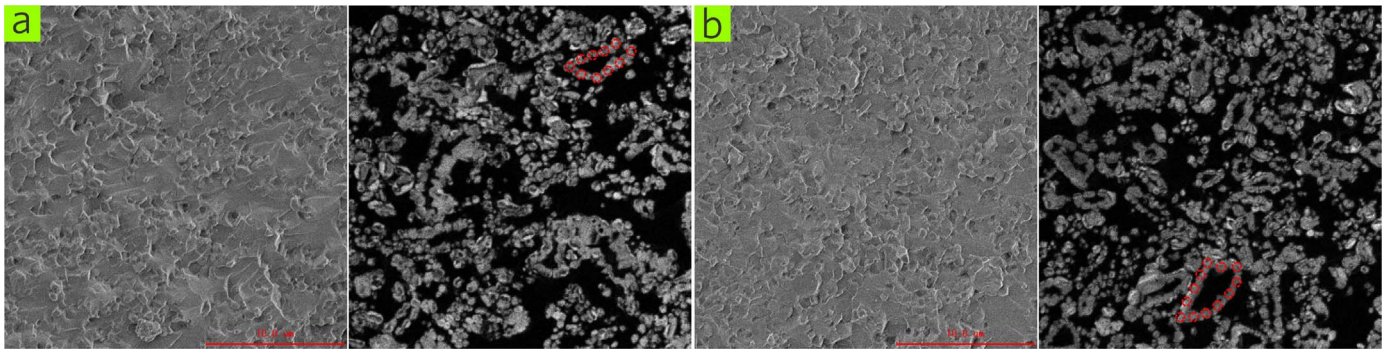

Fig. 2. SEM and corresponding CL mapping for 540 nm emission of samples a and c with cooling rate of 10 °C/min (a) and 1 °C/min (b), respectively. Scale bar is 10 μm. The spherical photoluminescent microcrystals generally tend to be arranged in a "necklace" pattern surrounding the inner non-luminescent glass phase (a representative one of such patterns is highlighted by red circles). (For interpretation of the references to color in this figure legend, the reader is referred to the web version of this article.)

intending to reveal the evolution of crystalline phases as well as the temperature threshold/range of obvious glass phase formation. As seen from Fig. 3a, the glass phase started to appear when the temperature was evaluated to be 1400 °C with the heating prolonged to be > 0.5 h (in sample g). Moreover, the amounts of the crystalline phases in the samples sintered at 1350 °C for 1 h, 1400 °C for 1 min, 0.5 h or 1 h, were roughly estimated, as listed in Table S1, and this evolution trend is illustrated in Fig. 3b. The main contribution of garnet phase formation is found to be the reaction between $Y_4Al_2O_9$, $BaAl_2Si_2O_8$ and $BaAl_2O_4$, as revealed from the comparison between the samples sintered at 1400 °C for 1 min and 0.5 h, respectively. Since the melting points for $BaAl_2Si_2O_8$ and $BaAl_2O_4$ have been reported as 1760 and 1815 °C, respectively [8,9], the composition of the glass at 1400 °C should be related with Ba-Si-Y-Al-O instead of either Ba-Si-Al-O or Ba-Al-O. Besides, it is more reasonable to interpret the composition of the garnet phase in a dynamic way: initially, the composition may be close to $Y_3Al_5O_{12}$; with gradual reaction between the garnet with $BaAl_2O_4$, $BaAl_2Si_2O_8$ and $Y_4Al_2O_9$, the composition of garnet will be getting closer to the derived $Y_2BaAl_4SiO_{12}$ garnet.

Based on all the above analysis, we propose the formation mechanism for the garnet phase, which should include an initial nucleation stage by conventional solid state reaction at a lower temperature and following liquid-assisted crystal growth at the higher temperature. The precipitation mechanism, even if it exists, does not contribute significantly. Such hypothesis can enable us to explain the microstructure feature that the luminescent microcrystals are being arranged in a "necklace" pattern surrounding the inner non-luminescent glass phase; besides, it can also explain the observed morphology feature of "core-shell" architecture within the individual microcrystals regarding emission intensity variation. As shown in Fig. 4b, the CL mapping (monitored for the 540 nm emission) of sample f (T=1400 °C, t=6 h, CR =5 °C/min) suggests the emission intensity is non-uniform within the individual crystals: the inner part of the crystals exhibit much lower brightness compared to the outer "shell"; thus, the content of Ce^{3+} ions successfully doped in the garnet lattice is much lower in the inner part compared to that in the outer "shell" part. Such feature can be explained by the two-stage hypothesis of "nucleation + crystal growth": when the nucleation begins at a relatively low temperature (< 1350 °C) by the conventional solid state reaction, the doping amount of Ce^{3+} into the garnet lattice is quite low due to a low activation energy/diffusion rate under low temperature; the amount of the garnet phase gets significantly increased at higher temperature with prolonged

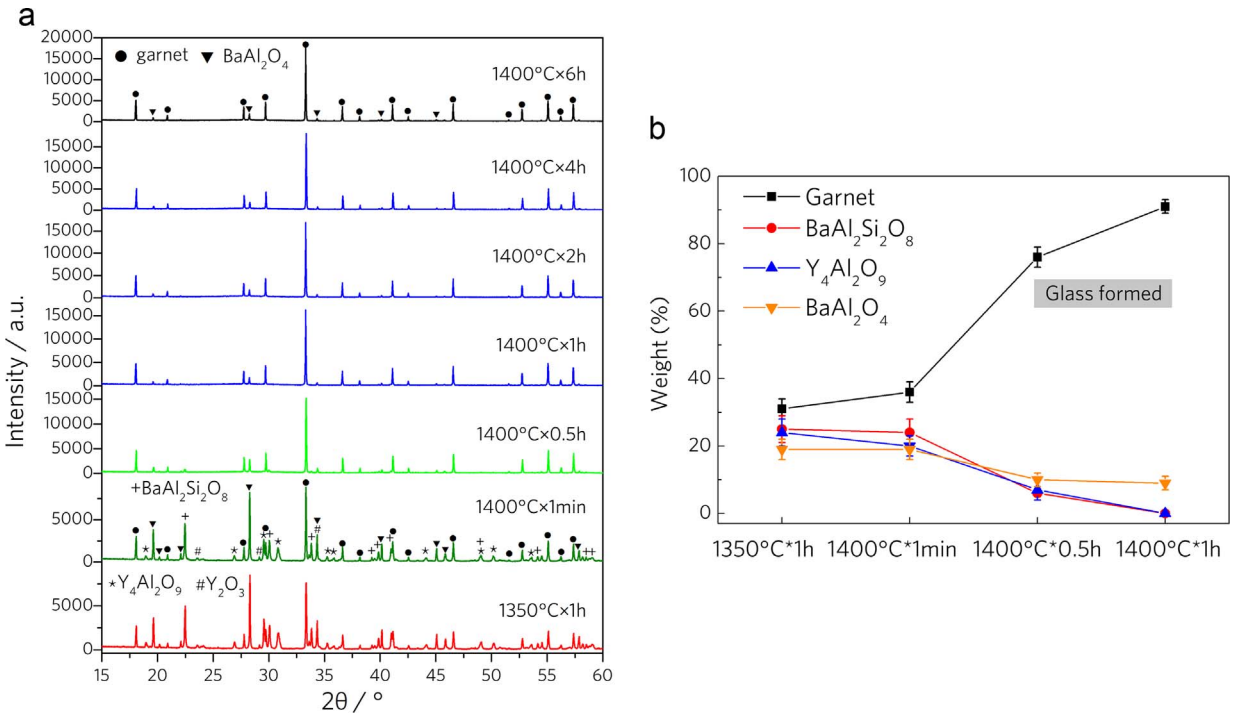

Fig. 3. (a) XRD patterns of the pellet samples sintered at 1350 or 1400 °C for 1 min, 0.5 h, 1 h, 2 h, 4 h, or 6 h. (b) Evolution of the crystalline phases in these samples.

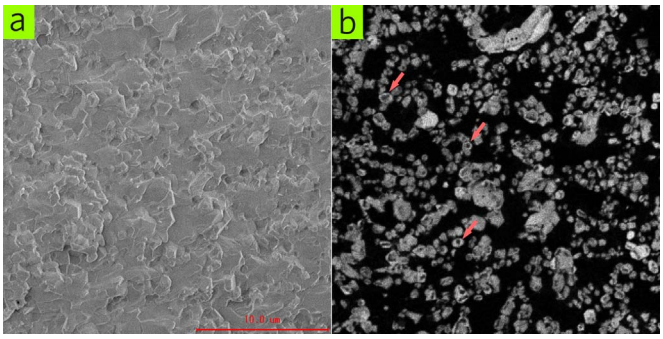

Fig. 4. SEM (a) and corresponding CL mapping for 540 nm emission (b) of the sample f (T=1400 °C, t=6 h). Scale bar is 10 μm. For individual luminescent garnet particles, a "core-shell" architecture regarding emission intensity variation is observed (such variations are representatively highlighted by pink arrows). (For interpretation of the references to color in this figure legend, the reader is referred to the web version of this article.)

heating period, and meanwhile, the occurrence of liquid phase greatly favors the diffusion reaction and also benefits for the Ce doping into the garnet, which then gives a high CL emission intensity.

A similar "core-shell architecture" phenomenon has been previously observed by us, when comparing the cross-sectional CL mapping between Ce^{3+}-doped $Lu_3Al_5O_{12}$ and $Lu_3(Al,Mg)_2(Al,Si)_3O_{12}$ phosphors: under a same synthesis condition, the pure $Lu_3Al_5O_{12}$:Ce shows "core-shell" feature regarding CL emission intensity variation (low emission intensity in the "core" and high emission intensity in the "shell"), while the Mg-Si pair doped ones show uniformly bright emission within the whole individual particles; the synthesis of these phosphors only involves with the conventional solid state reaction, and the difference in the occurrence of such "core-shell" feature is probably related to the Mg-Si favored diffusion rate of Ce into the host lattice or Mg-Si favored diffusion reaction between raw Lu_2O_3 and Al_2O_3. As for the Ce emission in the impurities, Pawade et al. [10] and Suriyamurthy et al. [11] respectively reported that Ce^{3+} in $BaAl_2Si_2O_8$ or $BaAl_2O_4$ exhibited blue emission band peaking at 442 nm (maximum excitation wavelength at 303 nm) or at 415 nm (maximum excitation wavelength at 350 nm). Since the CL spectrum at 442 or 415 nm gives quite low intensity [6], the Ce^{3+} may have not doped into the lattice of $BaAl_2O_4$ or $BaAl_2Si_2O_8$ in the present case; either Ce has preferable doping habit into the garnet lattice or some of Ce remains in the glass phase giving quite weak emission.

EDS mapping for a fractured surface in sample b was performed, as shown in Fig. 5. The fracture surface with both smooth and coarse feature was chosen, and as inspired from Fig. 4, they correspond to the glass and crystalline phases, respectively. It is seen that the Y, Ba, Al, Si elements clearly exhibit preferable distribution in these phases: Y and Al have similar distribution and tend to be in the crystalline phase, while Ba and Si are similarly distributed and concentrated in the glass phase. The O has a relatively uniform distribution within the whole fractured surface (if the effect of surface roughness was considered). Besides, the distribution of Y/Al in the glass phase (where Ba/Si are highly concentrated) is more demonstrated than that of Ba/Si in the crystalline phase (where Y/Al are highly concentrated). On one hand, this confirms that the glass phase has a composition related to Ba-Si-Y-Al-O; on the other hand, however, one may concern that whether or not the Ba/Si have been successfully incorporated into the crystalline phase or they are only retained in the glass phase. To verify this, a series sample of $Y_{2.96-x}Ce_{0.04}Ba_xAl_{5-x}Si_xO_{12}$ (x=0.6, 0.8, 1.0) were further prepared (powder sample; T=1400 °C, t=2 h, CR=5 °C/min) and their XRD patterns were subjected to Rietveld refinement. The evolution of the cell volume per x variation is shown in Fig. 6, which indicates a linear decreasing trend with Ba/Si gradually substituting for Y/Al. With coordination number of 8, Ba^{2+} and Y^{3+} have the effective ion radius of 1.42 and 1.019 Å, and with coordination number of 4, Si^{4+} and Al^{3+} have the effective ion radius of 0.26 and 0.39 Å [12]; the sum effect of Ba/Si replacing Y/Al causes contraction of the garnet unit cell, and the linear trend proves the successful pair substitution. Moreover, our previous Rietveld refinement on the XRD pattern of $Y_2BaAl_4SiO_{12}$ obtained satisfyingly low *R*-factors, which also justifies such derived garnet composition.

Synthesis of $Y_{1.82}Ce_{0.08}BaAl_4SiO_{12}$ pellet sample was further tried at 1450 °C for 2 h, in which the peak intensity of residue $BaAl_2O_4$ significantly decreased (Fig. 6b), compared with that sintered at 1400 °C (Fig. 3). The maximums of the PLE and PL spectra of the pellet phosphor are at 454 nm and 537 nm, respectively; full-width at half-maximum of the emission spectra is 104 nm (Fig. 6c). Since an advantage of the title phosphor is the relatively high emission stability against thermal quenching, follow-up studies can be the preparation of phosphor-in-glass convertor or transparent/translucent ceramic plate to seek for application in high power WLED.

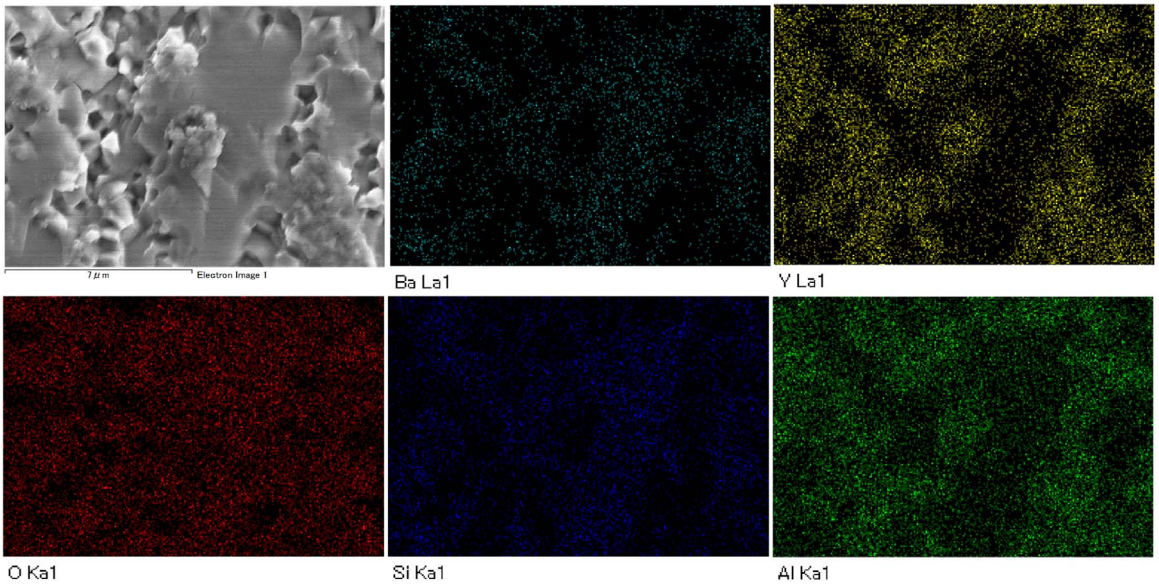

Fig. 5. EDS mapping for a fractured surface in the sample b (T=1400 °C, t=2 h). The smooth and coarse fracture features are related to the glass and crystalline phases, respectively. The Y/Al and Ba/Si elements show preferable distribution in these phases.

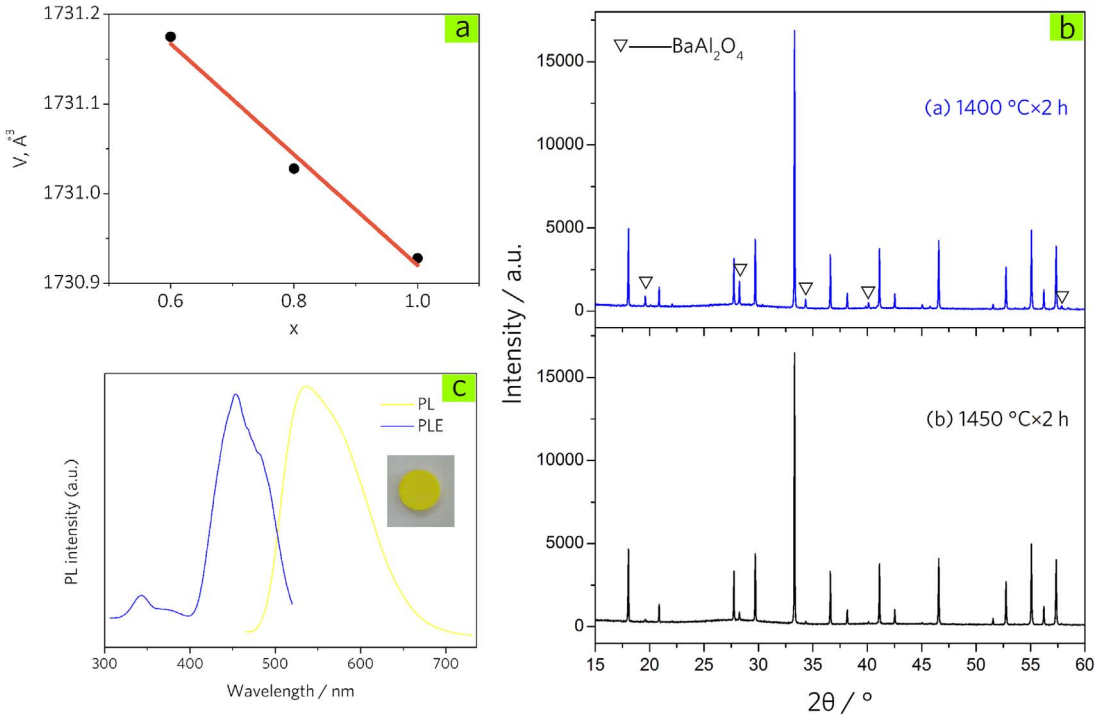

Fig. 6. (a) Cell volume per x in the samples with nominal compositions of $Y_{2.96-x}Ce_{0.04}Ba_xAl_{5-x}Si_xO_{12}$ (x=0.6, 0.8, 1.0). (b) XRD patterns of $Y_{1.82}Ce_{0.08}BaAl_4SiO_{12}$ pellets prepared at 1400 °C or 1450 °C for 2 h. (c) PLE and PL spectra of the $Y_{1.82}Ce_{0.08}BaAl_4SiO_{12}$ pellet sample (T=1450 °C, t=2 h, CR =5 °C/min). The insert shows the digital image of the as-prepared pellet phosphor.

4. Conclusions

The phase formation mechanism of the microcrystal-glass phosphor with nominal formula of $(Y,Ce)_2BaAl_4SiO_{12}$ were investigated by varying the synthesis parameters of heating temperature, holding period and cooling rate. The hypothesis of microcrystals precipitation from melt during heating/cooling was judged to have rarely contributed; instead, we propose a two-stage phase formation mechanism of an initial nucleation by solid state reaction at lower temperature and following growth by liquid-assisted diffusion/reaction at higher temperature. Such hypothesis enables us to explain the observed features including the “core-shell” architecture regarding cathodoluminescence emission intensity variation within individual luminescent microcrystals, as well as the arrangement of microcrystals around the glass phase forming a “necklace” pattern.

Acknowledgements

This study was partially supported by the National Natural Science Foundations of China (Grants No. 51272259, 51572232 and 51561135015). R.X. was partially supported by the JSPS KAKENHI (No. 15K06448). M.M. was partially supported by the Russian Foundation for Basic Research (Grant No. 15–52-53080) H.J. thanks the China Scholarship Council (CSC) for scholarship support.

Appendix A. Supplementary material

Supplementary data associated with this article can be found in the online version at http://dx.doi.org/10.1016/j.ceramint.2017.02.055.

References

[1] R.-J. Xie, H.T. Hintzen, Optical properties of (Oxy)Nitride materials: a Review, J. Am. Ceram. Soc. 96 (2013) 665–687.
[2] Z. Xia, A. Meijerink, Ce^{3+}-Doped garnet phosphors: composition modification, luminescence properties and applications, Chem. Soc. Rev. 46 (2017) 275–299.
[3] T. Zhou, L. Zhang, Z. Li, S. Wei, J. Wu, L. Wang, H. Yang, Z. Fu, H. Chen, D. Tang, C. Wong, Q. Zhang, Toward vacuum sintering of YAG transparent ceramic using divalent dopant as sintering aids: investigation of microstructural evolution and optical property, Ceram. Int. 43 (2017) 3140–3146.
[4] H. Ji, L. Wang, M.S. Molokeev, N. Hirosaki, R.-J. Xie, Z. Huang, Z. Xia, O.M. ten Kate, L. Liu, V.V. Atuchin, Structure evolution and photoluminescence of $Lu_3(Al,Mg)_2(Al,Si)_3O_{12}:Ce^{3+}$ phosphors: new yellow-color converters for blue LED-driven solid state lighting, J. Mater. Chem. C 4 (2016) 6855–6863.
[5] H. Ji, L. Wang, M. Molokeev, N. Hirosaki, Z. Huang, Z. Xia, O.M. ten Kate, L. Liu, R.-J. Xie, New garnet structure phosphors, $Lu_{3-x}Y_xMgAl_3SiO_{12}:Ce^{3+}$(x=0, 1, 2, 3), developed by solid solution design, J. Mater. Chem. C 4 (2016) 2359–2366.
[6] H. Ji, L. Wang, Y. Cho, N. Hirosaki, M. Molokeev, Z. Xia, Z. Huang, R.-J. Xie, New $Y_2BaAl_4SiO_{12}:Ce^{3+}$ yellow microcrystal-glass powder phosphor with high thermal emission stability, J. Mater. Chem. C 4 (2016) 9872–9878.
[7] TOPAS V4.2: General profile and structure analysis software for powder diffraction data - User’s Manual; Bruker AXS: Karlsruhe, Germany, 2008.
[8] W.E. Lee, M. Chen, P.F. James, Crystallization of Celsian ($BaAl_2Si_2O_8$) Glass, J. Am. Ceram. Soc. 78 (1995) 2180–2186.
[9] D. Jia, X.-j. Wang, E. van der Kolk, W.M. Yen, Site dependent thermoluminescence of long persistent phosphorescence of $BaAl_2O_4:Ce^{3+}$, Opt. Commun. 204 (2002) 247–251.
[10] V.B. Pawade, N.S. Dhoble, S.J. Dhoble, Rare earth (Eu^{2+},Ce^{3+}) activated $BaAl_2Si_2O_8$ blue emitting phosphor, J. Rare Earth 32 (2014) 593–597.
[11] N. Suriyamurthy, B.S. Panigrahi, Luminescence of $BaAl_2O_4:Mn^{2+}$,Ce^{3+} phosphor, J. Lumin 127 (2007) 483–488.
[12] R. Shannon, Revised effective ionic radii and systematic studies of interatomic distances in halides and chalcogenides, Acta Crystallogr. A 32 (1976) 751–767.